Journal of Applied Electrochemistry **34**: 919–927, 2004.
© 2004 *Kluwer Academic Publishers. Printed in the Netherlands.*

Investigation of the metal–oxide buried interfacial zone with linear sweep voltammetry

D.L. Cocke[1]*, D.E. Mencer[2], M.A. Hossain[1], R. Schennach[3], M. Kesmez[1], J.R. Parga[4] and D.G. Naugle[5]
[1]*Gill Chair of Chemistry and Chemical Engineering, Lamar University, Beaumont, TX 77710, USA*
[2]*Department of Chemistry, Wilkes University, Wilkes-Barre, PA 18776, USA*
[3]*Institute of Solid State Physics, Technical University of Graz, Austria*
[4]*Institute Technology of Saltillo, Department of Metallurgy and Materials Science, V. Carranza 2400, Saltillo Coah. Mexico, C.P. 25000*
[5]*Department of Physics, Texas A & M University, College Station, TX 77843, USA*
*(*author for correspondence, e-mail: cockedl@hal.lamar.edu)*

Received 26 June 2002; accepted in revised form 13 April 2004

Key words: copper, Cu_xO, Cu_2O, Cu_3O_2, CuO, oxide decomposition, oxygen diffusion, linear sweep voltammetry, modified Cabrera and Mott (C–M) model

Abstract

Interest in copper as a technologically important material needs to be met with greater understanding of the fundamental chemical reactions of copper. In particular, there is still a lack of universal agreement on the oxidation process of bulk copper and thin copper films. In this study, the authors demonstrate the use of linear sweep voltammetry (LSV) to study buried structures in the oxide layers on copper. In particular, LSV can be used to detect reactions at buried interfaces. It is also emphasized that surface scientists should recognize Cu_3O_2 and the decomposition of copper oxides at the metal–oxide interface in new studies on copper oxidation and in interpreting already existing copper oxidation data. The two key parameters that drive oxide growth and decomposition are demonstrated to be oxygen activity and the free energies of formation of the oxides (per mole of oxide ion). The complex nature of the oxidation of copper, as well as other metals and alloys, can be described qualitatively using the Modified Cabrera–Mott (C–M) Model. Surface studies of oxidation of metals and alloys need to be supported and complemented by other techniques such as chemical or electrochemical methods.

1. Introduction

A longstanding effort has been made by this group to understand the physical and chemical processes that control metal and alloy oxidation [1]. There is a continued interest in understanding low temperature (<200 °C) copper oxidation to improve the performance of copper components in the microelectronics industry. The oxides that form on copper at these temperatures can be chemically unstable and show mechanical instability if Cu^{2+} forms [2]. Despite the enormous number of techniques (surface enhanced Raman spectroscopy [3], RBS [4], ellipsometry [5], atom probe [6], and STM [7], pulsed field desorption mass spectrometry [8], XPS [2, 9–14], low angle X-ray diffraction [15], optical spectroscopy [9, 15–22], angle resolved XPS [23], and factor analysis and artificial neural network XPS depth profiling [24]) that have been used to explore the oxidation of copper, there remain open questions about the oxidation process and the oxide structure that forms under given conditions. There are recent studies of the low temperature oxidation of copper that fail to account for the complex nature of the oxide layers formed, the existence of Cu_3O_2, or the possibility of copper oxide decomposition at the metal–oxide interface [25–30]. In this manuscript the authors want to demonstrate that: (a) surface studies of alloy and metal oxidation need to be supported by chemical and electrochemical techniques, (b) Cu_3O_2 should be considered in interpreting new and prior studies on copper oxidation, and (c) oxide decomposition reactions at buried metal–oxide interfaces are crucial to understanding oxidation.

Wieder and Czanderna [18] delineated five oxide regions from room temperature to 330 °C during copper oxidation. These are seen in Figure 1 and are classified into different temperature regimes: (1) below 70 °C, (2) 70–110 °C, (3) 110–200 °C, (4) 200–270 °C, and (5) 270–330 °C. Region (1) is dominated by oxidative growth of an amorphous, or precursor, oxide. In both regions (2) and (4) dramatic compositional changes occur. The flat region (5) is due to cupric oxide, CuO, growth. Region (3) shows the unusual constant composition of $CuO_{0.67}$ (Cu_3O_2) rather than the expected $CuO_{0.5}$ (Cu_2O). This structure was optically characterized and shown to be

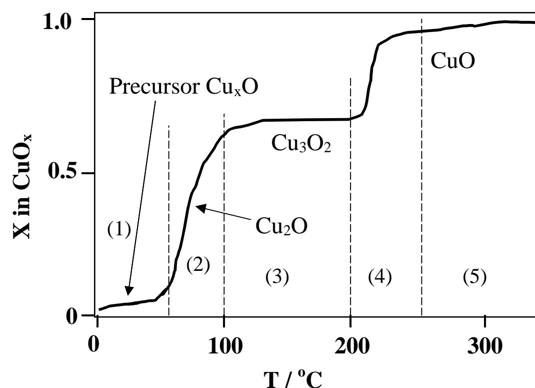

Fig. 1. Formation of different copper oxides as a function of temperature at a single P_{O_2} (after Czanderna [18]).

confined to a thickness of less than ~2400 Å by Wieder and Czanderna [31] and the composition confirmed in other studies [19–21]. Neumeister and Jaenicke [21] studied the effect of defects and found significant differences in the oxide growth depending on the history of the Cu sample. The proposed mechanism of Cu oxidation depends strongly on the amount of defects in Cu_2O, with an increase in the number of defects facilitating the formation of Cu_3O_2, a defect structure of Cu_2O. Eight reactions (see reactions 2–9 in Table 1) for the formation of copper oxide were proposed [21].

For Cu oxidized at 200 °C and 50 Torr O_2 they found initial formation of Cu_2O only (reaction 2). After oxidation of about 85% of the deposited Cu film, the Cu_2O changes almost completely to Cu_3O_2 (reactions 3 and 4) without the formation of CuO. Then oxidation of Cu_3O_2 to CuO starts on the outer surface of the Cu_3O_2 layer (reaction 5) but at the same time it decomposes to CuO and Cu_2O at the metal–oxide interface (reaction 9) allowing reaction of copper metal with CuO (reaction 7). After the Cu_3O_2 is used up, the oxidation continues slowly via the oxidation of Cu_2O and Cu to CuO (reactions 7 and 8). This study provided direct evidence for the presence of the Cu_3O_2 phase at these temperature and oxygen activity conditions. However, these eight reactions could also occur under different conditions.

More recent studies at modest temperatures and atmospheric pressure show that a precursor oxide with a Cu_2O structure forms but it contains Cu^0 [15]. This is in agreement with the work by Czanderna [18] and adds an initial oxidation step (reaction 1). After this precursor formation, the authors suggest that in the range of 100–200 °C, Cu_2O/Cu_3O_2 forms with Cu_3O_2 becoming more prevalent as the time of oxidation increases. Above 200 °C, CuO begins to form internally in the Cu_3O_2 phase. Yet at intermediate temperatures (150–250 °C) Lefez et al. [16] found that the oxidation progresses via rapid conversion of Cu to Cu_3O_2 along with slow formation of CuO as a result of internal vacancy aggregation in the Cu_3O_2. The final result is the formation of a multilayer/multiphase structure ($CuO/Cu_3O_2/Cu_2O/Cu$).

Other studies [12–16] have shown that the oxidation of copper may be more complicated than that indicated in Figure 1. Several groups have shown that the 'Cu_xO' structure (Stage 1 in Figure 1) developed at ambient temperature to 70 °C is at least a bilayer [16, 8, 10, 12, 15]. In an extensive examination of numerous metals, Barr [10] concluded that the precursor oxide is terminated by the highest oxidation state of the metal. In the case of copper, this is Cu^{2+} in an oxide/hydroxide form. Cocke and coworkers observed bilayer formation at 50 °C in pure oxygen and oxide instability during thermal annealing in a vacuum [12]. Apen et al. [2] have also examined the oxide formed at ambient conditions and found a bilayer structure. Cocke et al. [8] collected field desorption mass spectrum and clearly demonstrated the ion conductive properties of Cu_2O. It has been shown that this layer may have a variation in Cu/O ratio from the oxide-gas interface to the metal–oxide interface and that the layer contains Cu^0 [15]. This layer appears to persist into stage 2 and 3 oxidation (Figure 1) but appears to disappear in the stages 4 and 5 where CuO forms.

Stage 2 oxidation apparently produces Cu_2O over the precursor oxide Cu_xO [18], while stage 3 oxidation produces Cu_3O_2. Yet with the exception of the precursor oxide it has not been observed that Cu_2O exists below this layer [15, 16]. Oxidation in stage 4 produces CuO internally [15] and on the external surface while Cu_2O and Cu_3O_2 exist. Oxidation at 200 °C and above has been shown to produce at least three oxides: Cu_2O, Cu_3O_2 and CuO with the outer layer being a mixture of CuO and Cu(I) oxide [15]. Oxidation in stage 5 produces CuO over the lower copper oxides and Cu [10, 15, 18].

Table 1. Relevant reactions that can occur during the growth of oxide layers on copper under various conditions of temperature and oxygen pressure

Oxide formation reactions		Oxide decomposition reactions	
x Cu + 1/2 $O_2 \rightarrow Cu_xO$ (precursor)	(1)		
2 Cu + 1/2 $O_2 \rightarrow Cu_2O$	(2)		
3 Cu_2O + 1/2 $O_2 \rightarrow$ 2 Cu_3O_2	(3)		
3 Cu + $O_2 \rightarrow Cu_3O_2$	(4)		
Cu_3O_2 + 1/2 $O_2 \rightarrow$ 3 CuO	(5)	$Cu_3O_2 \rightarrow$ CuO + Cu_2O	(9)
Cu + CuO $\rightarrow Cu_2O$	(6)	2 CuO $\rightarrow$ 1/2 O_2 + Cu_2O	(10)
Cu_2O + 1/2 $O_2 \rightarrow$ 2 CuO	(7)	$Cu_xO \rightarrow O_{(abs)}$ + x Cu	(11)
Cu + 1/2 $O_2 \rightarrow$ CuO	(8)		

Note: These are the reactions that occur in dry oxygen, in the presence of water additional reactions may occur.

Cu_2O is cation-deficient and growth of Cu_2O involves cationic diffusion and p-type electronic conduction. At the metal–oxide interface, Cu^+ and electrons are produced:

$$Cu \rightarrow Cu^+ + e^- \quad (12)$$

Cations diffuse outward via vacant sites in the Cu^+ oxide lattice as electrons move out to the oxide–gas interface by positive-hole conduction to react with oxygen:

$$1/2\, O_2 + 2e^- \rightarrow O^{2-} \quad (13)$$

Therefore, the growth of the copper oxide is dependent upon the transport properties of the oxide layer and significant CuO formation in air or atmospheric pressures of oxygen is generally not observed until temperatures exceed 200 °C. The general wisdom developed after years of studies has been that formation of CuO, nonexistent below 150 °C, passes through a maximum at about 450 °C and decreases again at higher temperatures reaching a minima above 900 °C [32].

In this paper the authors propose an important addition to the oxidation mechanisms discussed above. The additional steps involve oxide decomposition processes that occur at the buried metal–oxide interface (see Table 1). Evidence for these processes is provided from prior X-ray photoelectron spectroscopy (XPS) and Pulsed Field Desorption Mass Spectrometry studies. Additionally, new evidence for the oxide decomposition process is provided by linear sweep voltammetry (LSV) studies. Figure 2 shows the linear sweep voltammagrams from two copper oxide overlayers grown in air (a) for 60 min at 50 °C, (b) for 60 min at 150 °C, and (c) a native oxide layer grown at ambient temperature. The key point to be noted at this time is the appearance of a very easily reduced species (labeled metal–oxide interfacial zone) in Figure 2 curve (b).

2. Experimental

Copper discs (1 mm thick by 1 cm dia.) were cut from oxygen free high conductivity (OFHC) copper rod ($\geqslant$99.95%). The discs were wet polished in alternating directions by hand with 220, 320, 400, 600 and 1500 grit silicon carbide sandpaper. The polished discs were rinsed with water (Aldrich 99.5+%, A.C.S., reagent), isopropyl alcohol (LabChem Inc. 70% v/v), and water again followed by daubing dry on laboratory wipes. Oxidation was accomplished by placing the samples on a preheated iron block in a laboratory oven at 50, 75, 150, 250 and 300 °C in air for various lengths of time (1–5 min, 10 min, 20 min, 30 min, 1 h, 3 h, up to 25 h). Linear sweep voltammetry was carried out using Solartron 1280B electrochemical measurement unit interfaced with a PC. The backside of the copper disks were cleaned with emery paper to ensure electrical contact, samples were analyzed in pH 9.18 sodium tetraborate buffer and were nitrogen purged in order to minimize oxygen content. All voltages are referenced to a saturated Ag/AgCl electrode and shifted to a common onset of hydrogen evolution to facilitate comparison of oxide layers of different thicknesses. The LSV experimental procedure can be found in a previous paper [33].

3. Results

The LSV for an ambient 'native oxide' layer comprises of a surface oxide layer that is composed of at least two components (Figure 2c). This layer consists of the 'precursor oxide' (major peak at ca. −0.47 V) and terminating layer of CuO or $Cu(OH)_2$ (very low shoulder at ca. −0.59 V). The terminating layer of Cu^{2+} species was confirmed with XPS (Mencer et al., in preparation). When comparing the samples prepared by thermal oxidation at low, 50 °C (Figure 2a), and medium,

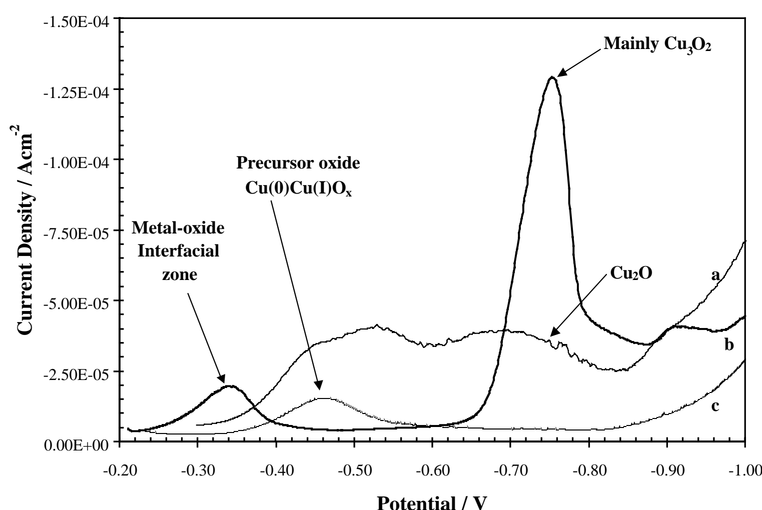

Fig. 2. Linear sweep volatmmograms (in pH 9.18 buffer solution) of copper oxide layers grown in air (a) for 60 min at 50 °C, (b) for 60 min at 150 °C and (c) at ambient temperatures.

150 °C (Figure 2b), other obvious differences appear in the LSV data. The 50 °C (1 h) data provides evidence for the 'precursor oxide' (at ca. −0.50 V) and for the growth of Cu_2O (at ca. −0.70 V). The outermost layer of this sample should also contain some CuO or $Cu(OH)_2$ as has been demonstrated previously by XPS [10].

The 150 °C (1 h) data has no peak at ca. −0.50 V demonstrating the disappearance of the 'precursor oxide' along with the growth of Cu_3O_2. Due to increasing oxide thickness, the peaks for the oxide components have been shifted to more negative potentials due to IR drop across the oxide. More critically the data at 150 °C includes a new easily reducible species as seen by the presence of the peak at approximately −0.34 V. It is notable that the appearance of this species is coupled with the disappearance of the precursor oxide peak. At 150 °C in air the precursor peak is present after oxidation for 1, 2, 3, 4, 5, 10, and 20 min but disappears after 30 min and does not return. The authors conclude that the changes in these peaks provide direct evidence for copper oxide decomposition at the metal–oxide interface (reaction 11 in Table 1).

The minimum time required for the appearance of the 'metal–oxide interfacial zone' peak decreases with increasing temperature, as shown in Figure 3, suggesting kinetic control. Oxide layers grown for a period of 25 h at 50 or 75 °C (Figure 3a, b) lack this highly reducible species. However, the peak appears after 30 min at 150 °C (Figure 3c), after 4 min at 250 °C (Figure 3d) and after only 1 min at 300 °C (Figure 3e). The coupling of the appearance of the 'metal–oxide interfacial zone' peak with the disappearance of the precursor oxide peak is informative. It appears that this LSV data provides good evidence for the growth of copper oxides above a precursor layer (by cationic conduction), followed by the decomposition of the precursor oxide (at the buried metal–oxide interface) when the temperature reaches some minimum value between 75 and 150 °C.

4. Discussion

In spite of the better control over producing specific oxides at low pressure and controlled temperatures conditions when doing *in situ* surface analysis studies, a strong case can be made that additional techniques can give supporting data on the chemical nature and structure of the oxide films grown on metals and alloys. Surface analyses of copper oxides have been supported by experiments using other methods including optical [9, 15–22], RBS [4], electrochemical methods, and even chemical methods [34]. Bubert [34] determined the surface oxygen content by carrier-gas fusion analysis and the copper content was determined by selective dissolution of the oxide layers using NH_4OH–NH_4Cl. This method provides some insight on the oxide thickness but little about its chemical nature. On the other hand, LSV is an electrochemical method that can provide information about the chemical nature of the oxides formed on metal substrates. Peak position in LSV depends on the reducibility of the oxide and on the IR drop. Oxide layers formed of different oxides show reduction peaks at different potentials and it is possible to detect very small structures with LSV. Deconvolution of LSV data [35–37] obtained from copper oxide grown at ambient temperature in oxygen plasma provided evidence for five types of oxides in the LSV data: a precursor oxide (Cu_xO), CuO, Cu^+ (hydrated oxide or hydroxide), Cu_3O_2 and Cu_2O. The Cu^+ (hydrated oxide or hydroxide) is formed after the initial reduction of CuO and occurs more readily than the reduction of the thermally grown Cu_2O [17, 38]. The reduction potentials are in agreement with a prior study [17] in which no distinction was made between Cu_3O_2 and Cu_2O. Figures 2 and 3 clearly demonstrate that the decomposition of the precursor oxide at the metal–oxide interface is of critical importance in the oxidation of copper at intermediate temperatures (75–150 °C).

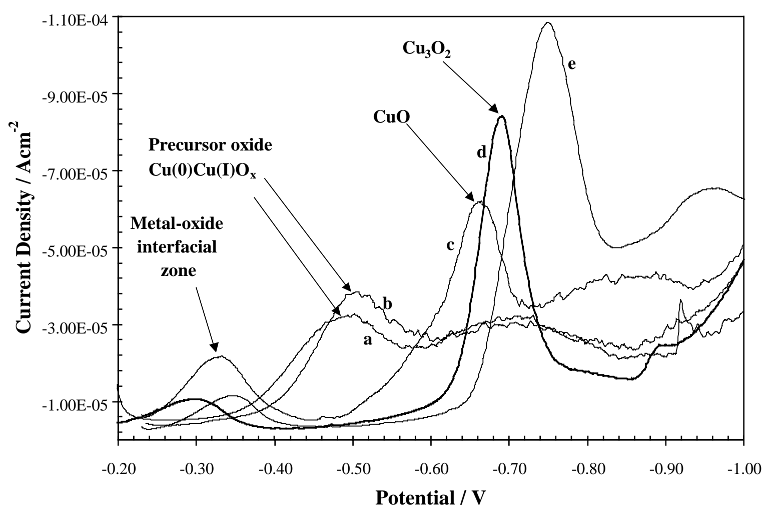

Fig. 3. Linear sweep voltammograms (in pH 9.18 buffer solution) of copper oxide layers grown in air (a) for 25 h at 50 °C, (b) for 25 h at 75 °C, (c) for 30 min at 150 °C, (d) for 4 min at 250 °C and (e) 1 min at 300 °C. The current density of curve (e) was multiplied by 0.5.

Studies of thermal oxidation of Cu–Mn [11], Ag–Mn [39], Ni–Zr [40–42], Ni–Ti [43], Ni–Hf [44], Ti–Cu [45, 46] and Ti–Al [45, 47] have helped to better understand the parameters that control metal and alloy oxidation. The chemical reaction between a metal, M, and gaseous oxygen is

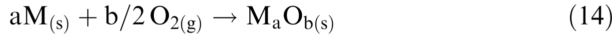

$$aM_{(s)} + b/2\,O_{2(g)} \rightarrow M_aO_{b(s)} \tag{14}$$

and can be divided into nine steps (refer to Table 2) as proposed by Bailey and Ritchie [48, 49]. Building on that model it is relatively simple to demonstrate that oxidation can be discussed in terms of the modified Cabrera and Mott (C–M) model. The C–M model has been reviewed by both Parkhutik [50] and Cocke [1] and can be explained through discussion of the following equation:

$$\Delta\Phi = \frac{-\Delta G_{\mathrm{f}}^{0}}{2\mathrm{e}} + \frac{kT}{2\mathrm{e}}\ln\left[\frac{4\mathrm{e}^2 N_{\mathrm{s}}(\mathrm{aO_2})^{1/2}x}{kT\varepsilon\varepsilon_0}\right] \tag{15}$$

$\Delta\Phi$ is the potential that develops across a growing oxide, $-\Delta G_{\mathrm{f}}^{0}$ is the free energy of formation of oxygen anions at the surface (approximated by the free energy of formation of the oxide per mole of O^{2-}), plus a functional term of temperature (T), the total number of surface O^{2-} ions in unit surface area (N_{s}), oxygen activity (aO_2), film thickness (x), electronic charge (e), the dielectric constant (ε), and dielectric constant in vacuum (ε_0). However, in cases where more than one oxide forms, the model must be modified in order to predict the total potential that controls oxide growth. Considering the total potential as the sum of the potentials for each oxide of each metal component, $\Delta\Phi = \Delta\Phi_{M_1} + \Delta\Phi_{M_2} + \cdots$ leads to the following expression:

$$\Delta\Phi = \frac{-\Delta G^{0}_{\mathrm{f}_{M_1}}}{2b\mathrm{e}^-} + \frac{kT}{2b\mathrm{e}^-}\ln\left[\frac{(2b\mathrm{e}^-)^{\mathrm{b}} N_{\mathrm{S}}^{\mathrm{b}} a_{\mathrm{O_2}}^{\mathrm{b}/2} a_{M_1}^{\mathrm{a}} X^{\mathrm{b}}}{kT\varepsilon^{\mathrm{b}}\varepsilon_0^{\mathrm{b}} a^{\mathrm{a}}_{M_1^{2\mathrm{b/a}}}}\right] + \frac{-\Delta G^{0}_{\mathrm{f}_{M_2}}}{2d\mathrm{e}^-} + \frac{kT}{2d\mathrm{e}^-}\ln\left[\frac{(2d\mathrm{e}^-)^{\mathrm{d}} N_{\mathrm{S}}^{\mathrm{d}} a_{\mathrm{O_2}}^{\mathrm{d}/2} a_{M_2}^{\mathrm{c}} X^{\mathrm{d}}}{kT\varepsilon^{\mathrm{d}}\varepsilon_0^{\mathrm{d}} a^{\mathrm{c}}_{M_2^{2\mathrm{d/c}}}}\right] + \cdots \tag{16}$$

The terms in Equation (16) are: the free energies of oxide formation per mole of O^{2-} ($-\Delta G^{0}_{\mathrm{f}_{M_x}}$) for the particular metal oxide, the stoichiometric factors from the oxidation reactions (a, b for M_1 and c, d for M_2), the oxygen, metal and metal ion activities (a_x), and the other parameters as discussed for Equation (15). At any given temperature and partial pressure of oxygen, the oxide growth is dependent on the oxide thickness and the value of the free energy terms. However, oxidation in alloys will also vary as a function of alloy composition.

In the absence of bulk diffusion limitations, the rate-controlling process is commonly thought to be the injection of a defect into the oxide at either the metal–oxide or the oxide–gas interface. However, with the complicated nature of the oxide layer on metals, as illustrated by copper in this paper, the buried interfaces and subsurface phases can have substantial and as yet poorly understood influences. The plot in Figure 1 is in relatively good agreement with the predictions of the modified C–M model. Here, the precursor oxide forms first, the Cu_2O forms next, followed by Cu_3O_2 and finally CuO forms. This is in the expected order of the free energies of formation of the oxides [1].

Prior studies with PFDMS also showed the predicted order of oxide formation [8]. In the original publication, Cocke et al. assigned the PFDMS spectra as follows: (a) Cu_2O for the oxide grown at room temperature, (b) a

Table 2. Nine electrochemical steps in the overall reaction (reaction 14) [48, 49]

Step no. (s)	Step	Stoichiometric # v_s
7	$M \rightarrow (M^{z+}\|M) + z^+e_M$	a
1	$e_M \rightarrow e_O$	az$^+$
2	$(M^{z+}\|M) + \Delta_O \rightarrow (M^{z+}\|\Delta)_O$	a
3	$e_O \rightarrow e_L$	az$^+$
4	$(M^{z+}\|\Delta)_O + \Delta_L \rightarrow (M^{z+}\|\Delta)_L + \Delta_O$	a
8	$O_{2\,(g)} + S \rightarrow (O_2\|S)$	b/2
5	$4\,e_L + (O_2\|S) + S \rightarrow 2(O^{2-}\|S)$	b/2
6	$(M^{z+}\|\Delta)_L + S' \rightarrow (M^{z+}\|S') + \Delta_L$	a
9	$a\,(M^{z+}\|S') + b\,(O^{2-}\|S) \rightarrow M_aO_b + aS' + bS$	1

List of symbols used:

- M represents a metal atom that reacts with O_2 in the ratio a : b/2 to form the oxide M_aO_b
- $(M^{z+}|M)$ represents a metal cation of charge z^+ e situated at the metal–oxide interface
- e represents the magnitude of electronic charge of an electron
- $(M^{z+}|\Delta)$ represents a cation on an interstitial site Δ within the oxide
- $(M^{z+}|S')$ represents a cation at a surface site S′ on the oxide–oxygen interface
- $(O_2|S)$ and $(O^{2-}|S)$ represent an oxygen molecule and an oxide ion, respectively, adsorbed at a site S on the oxide–oxygen surface
- and the subscripts M, O, L indicate the metal at the metal–oxide interface and the oxide at the metal–oxide (x = 0) and oxide (x = L), interface, respectively.

The stoichiometric numbers (i.e., the number of times that step s must occur for the formation of one molecule of M_aO_b) are given by v_s.

CuO layer over a Cu_2O for the oxide grown at 50 °C and 10^{-2} Torr O_2, and (c) CuO for the oxide grown at 200 °C and 1 atm O_2. These assignments of copper oxide speciation were based on XPS results that showed that Cu^{2+} was present in the overlayer for the oxide grown at 50 °C and as CuO for the oxide grown at 200 °C. However, there was no explanation for the differences seen in the PFDMS spectra for the Cu^{2+} found at both 50 and 200 °C and both had been tentatively assigned to CuO. Since Cu_3O_2 has one Cu^{2+} ion for every three Cu^+ ion in its unit cell, it is likely that the overlayer grown at 50 °C and 10^{-2} Torr O_2 was indeed Cu_3O_2. This is supported by the fact that the relative Cu^+ ion intensity was higher than that found for CuO in the sample grown at 200 °C. In fact, the presence of Cu^+ intensity in the sample grown at 200 °C provides additional evidence for the multilayer/multiphase structure discussed above ($CuO/Cu_3O_2/Cu_2O/Cu$).

As seen from the discussion above, thermal oxidation of copper at atmospheric pressure or reduced pressures produces, depending on the temperature, complex oxide structures. The dependence of copper oxidation on the pressure was demonstrated for the oxygen pressure range from 5×10^{-7} Torr up to 2 Torr at 250 °C [51]. Evidence from the O 1s XPS, the Cu 2p, and the Cu (L_3VV) Auger signal led to the following conclusions. The Cu (L_3VV) Auger signal shows only Cu^0 up to an oxygen pressure of 0.02 Torr. Significant surface oxide signal (O 1s) only begins to appear on at an oxygen pressure of 0.2 Torr. At this oxygen pressure, the Cu Auger peak shifts to a smaller kinetic energy indicating the appearance of Cu^+. This indicates the formation of Cu_2O at 250 °C and 0.2 Torr oxygen. Only when oxygen pressure reached 2 Torr was a small increase in the copper 2p XPS (high binding energy) signal detected indicating the formation of Cu^{2+} [51]. However, the Cu Auger signal at this pressure still shows a significant amount of Cu^+. Low take-off angle measurements were performed that displayed no enhancement of the Cu^{2+} signal at low angles. This observation is consistent with the formation of Cu_3O_2 under these oxidation conditions. This suggests that in the presence of sufficient oxygen, and in the absence of water, Cu_3O_2 is a major component in the oxide formed below 200–250 °C. At atmospheric pressure and 250 °C mainly CuO is formed [13, 18] (Mencer et al., in preparation). However, at low oxygen activity the processes occurring at the buried metal–oxide interface must be considered.

It is known that on all crystal faces examined to date, oxygen undergoes dissociative adsorption on copper. According to the hole theory developed by Delchar and Tompkins [52], random vibrations can produce a concerted motion of three or four adjacent surface metal atoms allowing entry of an adsorbed oxygen atom into the metal lattice over a reduced energy barrier. Srinivasan et al. [53] attributed an unusually low binding energy state of oxygen on copper (529.0 eV) to oxygen incorporated into the copper subsurface lattice. This interpretation was supported by the results of Lao et al. [54], Braithwaite et al. [55], and by early studies of polycrystalline copper surfaces by work function and adsorption techniques showing that this process is facilitated at higher oxygen pressure. However, the current study deals with oxide layers and not dissociatively adsorbed oxygen.

Yoon has also demonstrated that Cu_2O decomposes to form metallic copper in low oxygen pressure (4×10^{-3} Pa or 3×10^{-5} Torr O_2) when heated for 30 min at temperatures from 30 to 260 °C [12, 51]. In Figure 4A, the O 1s region is shown illustrating the presence of both chemisorbed and oxide species at low temperatures (curves a–c). At higher temperatures, the oxide peak is substantially reduced (curves d–g). The data in Figure 4B shows that the loss of the oxide peak is coupled with a conversion of Cu^+ to Cu^0 as indicated by the shift in the Cu L_3VV peak. The authors explained that two processes were involved in this change. First Cu^+ is

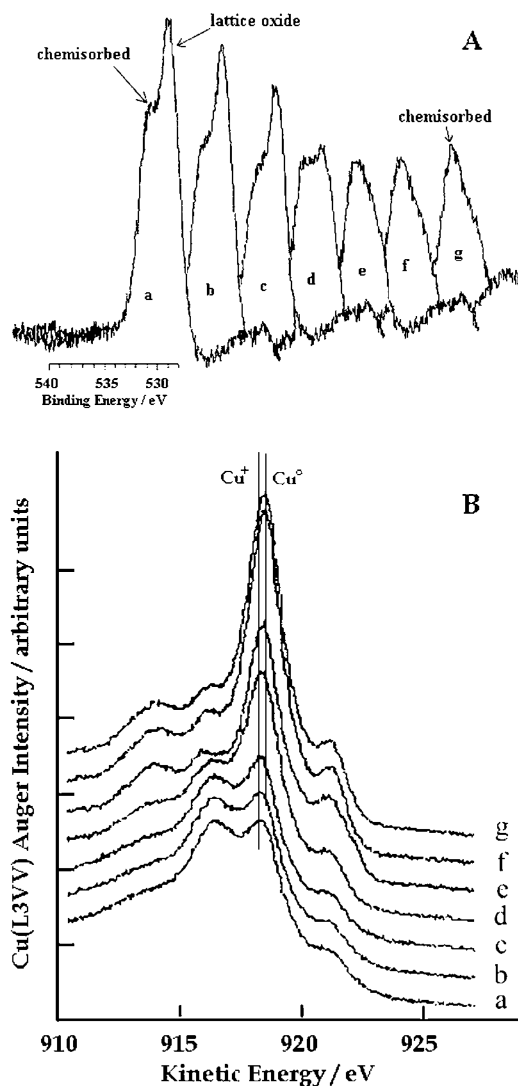

Fig. 4. (A) The O 1s XPS and (B) Cu (L_3VV) Auger spectra of copper after treatments for 30 min at 3×10^{-5} Torr as a function of temperature: (a) 30 °C, (b) 50 °C, (c) 80 °C, (d) 140 °C, (e) 190 °C, (f) 230 °C, and (g) 260 °C (after Yoon et al. [12, 51]).

reduced and oxide ions, O^{2-}, are oxidized followed by the absorption of the neutral oxygen species into the copper lattice. This process is kinetically controlled and does not occur until the temperature reaches approximately 110–140 °C. The authors of this study would like to propose that the same oxide decomposition occurs at higher oxygen pressures if the effective oxygen activity at the metal–oxide interface is low enough. This certainly can occur in cases where the oxide layer thickens and transport of ions becomes a limiting factor for oxide formation. The relevant reaction is the decomposition of the precursor oxide at the metal–oxide interface (see reaction 11 in Table 1). This results in oxygen absorbed in the copper lattice. The LSV data in the current study definitely support the presence of a very highly reducible species at ca. −0.34 V (Figures 2 and 3). If atomic oxygen is absorbed within the copper lattice, it would be easily reduced to O^{2-} and driven from the lattice through the overlying oxide layer by the negative potential applied to the copper cathode. Once at the oxide-solution interface it could react with water to form hydroxide. The process could be shown as follows:

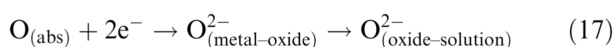

$$O_{(abs)} + 2e^- \rightarrow O^{2-}_{(metal\text{–}oxide)} \rightarrow O^{2-}_{(oxide\text{–}solution)} \quad (17)$$

$$H_2O + O^{2-}_{(oxide\text{–}solution)} \rightarrow 2OH^- \quad (18)$$

The question arises as to what the value of x is in the precursor oxide, Cu_xO. Certainly $x > 2$ since the precursor oxide is not Cu_2O, but rather Cu_2O with metallic copper atoms [17]. Other researchers report the presence of Cu_xO with $x > 4$ during the growth of oxide layers on copper [38]. However, the numerical value of x is probably best interpreted as being variable in agreement with the early work of Czanderna [18]. A rough schematic representation of the complex oxide structures formed during copper oxidation is shown in Figure 5. Note that the oxygen produced in reaction 11 is absorbed oxygen incorporated into the copper lattice. Figure 5a illustrates the oxidation processes expected at atmospheric pressure in air. This series of figures include the formation of a nonstoichiometric precursor oxide species at low temperatures (stages 1–2) that has been discussed by others [15], the growth of Cu_3O_2 (beginning in stage 3) and most critically the oxide decomposition reactions that can occur at the buried metal–oxide interface (stages 3–5). The precursor oxide is absent in stages 3–5 while the metal–oxide interfacial zone involving an absorbed oxygen species is present. In stage 4, Cu_3O_2 is consumed being converted into Cu_2O through reaction 9. Finally in stage 5 CuO increases in abundance while the other oxide persist beneath this layer. Figure 5b illustrates the dramatic effect pressure can have on the growth of oxides on copper. At a pressure of 2×10^{-2} Torr copper does not begin to show signs of

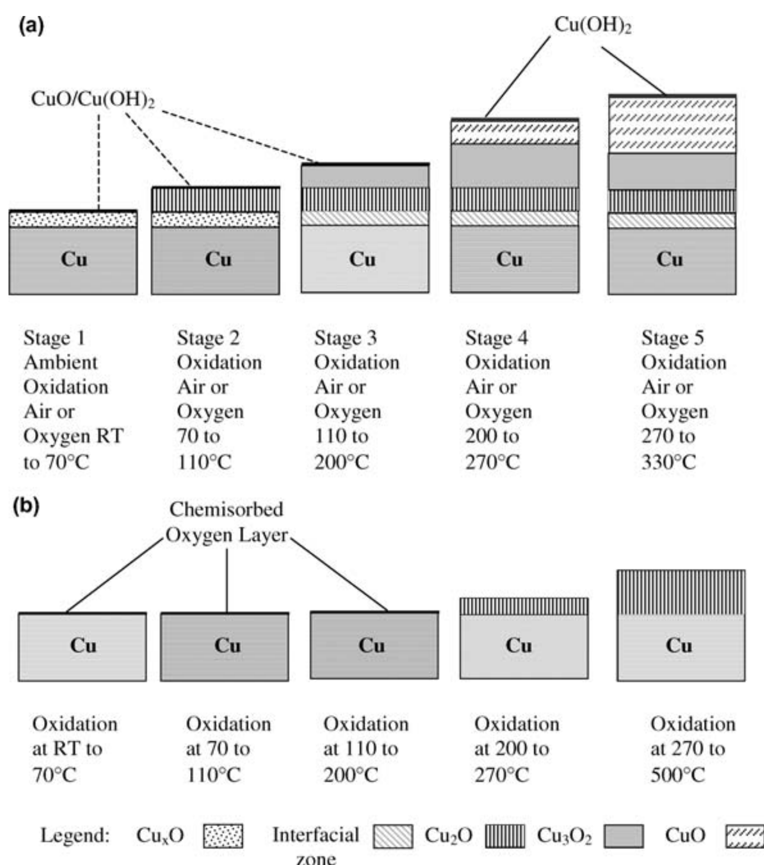

Fig. 5. A schematic of the complex oxide layer structures that form on Cu during oxidation at (a) atmospheric and (b) low oxygen pressure, 2×10^{-2} Torr (refer to text for discussion).

oxidation until at least 200 °C with oxide growth becoming significant at 300 °C and continuing to 500 °C [51].

The series of reactions in Table 1 are proposed to explain the processes that occur during each stage of oxide growth. The reaction scheme includes oxide growth processes and oxide decomposition processes. It is imperative to recognize that the specification of oxide growth parameters include not only temperature but also length of time (related to oxide thickness) and oxygen pressure. In fact it is more appropriate to consider effective oxygen activities found within the buried structures of the oxide overlayer. It should be noted that no clear-cut temperature ranges can be specified for the reactions listed in the absence of pressure specifications. CuO can easily decompose into Cu_2O (reaction 10) at many temperatures. At atmospheric pressure, CuO is most stable at about 450 °C. It should also be noted that reaction 11 in Table 1 occurs over a wide range of temperatures greater than approximately 110 °C. For oxide films grown on thin films of copper, the amount of oxygen that could be generated by decomposition of the precursor oxide could exceed the ability of the copper lattice to absorb the atomic oxygen. However, the precursor oxide decomposition process may be coupled with the diffusion of oxygen to the surface where it can be desorbed (or reacted again to form oxide ions to grow additional oxide at the oxide–gas interface).

Oxide decomposition has also been observed for silver and manganese oxides in AgMn alloys [39, 46], and for titanium oxides in samples of Ti, Ti_3 Al, TiAl, and $TiAl_3$ [45, 47, 56] treated at elevated temperatures in lower oxygen pressures or in vacuum (approximately 1×10^{-6} Torr). The work on the titanium aluminum alloys indicates that high diffusivity of oxygen into the metal is an important parameter. For the aluminum rich alloy, $TiAl_3$, the higher oxides of titanium were less prone to decomposition due to the lower oxygen diffusivity into aluminum vs. titanium. This argument was further supported by experiments in which a diffusion barrier, an intervening gold layer, was deposited between the OFHC copper substrate and the titanium film [57]. The titanium oxidized more rapidly and was less prone to decomposition of the higher oxides at high temperatures on the gold-coated substrate. Oxygen activity and oxide decomposition reactions should be considered when developing models of oxide growth.

Oxide decomposition reactions can also be interpreted using the modified C–M model. When the oxygen activity is low, as it will be at an oxide–vacuum interface or at a buried metal–oxide interface, an oxide can decompose (i.e. the oxide formation becomes the thermodynamically unfavorable process). The oxide must have a low enough free energy of formation to permit the reverse reaction to occur and there must be a means to dissipate the oxygen. Oxide decomposition should be observed for the more noble metals and in cases where oxygen solubility in the metal is high. Thus, the C–M model can play a useful role in predicting oxide growth mechanisms, and it can also be used to describe oxide decomposition reactions at low oxygen activity.

5. Conclusion

Future studies of the oxide layers developed on copper need to consider the presence of Cu_3O_2 and in the appropriate temperature and pressure regions, the decomposition of oxides at the metal–oxide interface. Additional studies in which oxygen pressure, temperature and time are used as effective parameters to better control the oxide growth must be combined with surface analysis and electrochemical tools to better characterize the oxides that form. Electrochemical methods can be of substantial help in delineating the complex nature of copper oxides formed under different oxidation conditions. The modified model of Cabrera and Mott is a useful tool for the prediction and explanation of the oxidation process of single metals and alloys. It should be used to guide further experimentation into the growth processes of oxides on copper and other metallic systems.

Acknowledgement

This work was supported primarily by the Robert A. Welch Foundation (Houston, TX) under Grant No. V-1103 and Welch Grant # A-0514, the Gulf Coast Hazardous Substance Research Center under Grant No. EPA-118LUB3653, the Texas Hazardous Waste Research Center under Grant No. 0669LUB0745, and the Texas Air Research Center under Grant Nos. 129LUB001A and 2001LUB2001A. This material is based in part upon work supported by the Texas Advanced Technology Program under Grant No. 003581-0013-1999.

References

1. D.L. Cocke, in Proceedings of XXII Congresso Internaciaonal de Metalurgia y Materiales, November 2000, (Instituto Technologico de Saltillo, Saltillo, Coahuila, Mexico) p. xiv.
2. E. Apen, B.R. Rogers and J.A. Sellers, *J. Vac. Sci. Technol.* **16** (1998) 1227.
3. H.Y.H. Chan, C.G. Takoudis and M.J. Weaver, *Electrochem. Solid State Lett.* **2** (1999) 189.
4. J. Li, J.W. Mayer and E.G. Colgan, *J. Appl. Phys.* **70** (1991) 2820.
5. M. Rauh and P. Wissmann, *Thin Solid Films* **228** (1993) 121.
6. K. Hono, H. Pickering, T. Hashizume, I. Kamiya and T. Sakurai, *Surf. Sci.* **213** (1989) 90.
7. R. Garcia-Cantu, J.J. Alvarado and O. Solorza, *J. Microsc.* **171** (1993) 167.
8. D.L. Cocke, G.K. Chuah, N. Kruse and J.H. Block, *Appl. Sur. Sci.* **84** (1995) 153.
9. J.M. Machefert, M. Lenglet, D. Blavette, A. Menard and A. D'Huysser, 'Structure and Reactivity of Surfaces' (Elsevier, Amsterdam, 1989) p. 625.
10. T. Barr, *J. Phys. Chem.* **82** (1978) 1801.

11. C. Yoon and D.L. Cocke, *Appl. Surf. Sci.* **31** (1988) 118.
12. C.H. Yoon and D.L. Cocke, *J. Electrochem. Soc.* **134** (1987) 643.
13. H. Streblow and B. Titze, *Electrochim. Acta* **25** (1980) 839.
14. G.N. Raikar, J.C. Gregory and P.N. Peters, *Oxid. Met.* **42** (1994) 1.
15. M. Lenglet, K. Kartouni, J. Machefert, J.M. Claude, P. Steinmetz, E. Beauprez, J. Heinrich and N. Celati, *Mat. Res. Bull.* **30** (1995) 393.
16. B. Lefez, K. Kartouni, M. Lenglet, D. Ronnow and C. G. Ribbing, *Surf. Int. Anal.* **22** (1994) 451.
17. M. Lenglet, K. Kartouni and D. Delehaye, *J. Appl. Electrochem.* **21** (1991) 697.
18. H. Weider and A. W. Czanderna, *J. Phys. Chem.* **28** (1962) 816.
19. E.G. Clarke and A.W. Czanderna, *Surf. Sci.* **49** (1975) 529.
20. M.G. Hapse, M.K. Gharpurey and A.B. Biswas, *Surf. Sci.* **9** (1968) 87.
21. H. Neumeister and W. Jaenicke, *Z. Phys Chem. Neue Folge* **108** (1978) 217.
22. A.W. Czanderna and H. Wieder, in R.F. Walker (Ed), 'Vacuum Microbalance Techniques', Vol. 2 (Plenum Press, Inc., New York, 1962) p. 147.
23. S. Suzuki, Y. Ishikawa, M. Isshiki and Y. Wsaeda, *Mater. Trans. JIM* **38** (1997) 1004.
24. H. Bubert and T. Appel, *J. Microsc. Soc. Am.* **2** (1996) 35.
25. M. O'Reilly, X. Jaing, J.T. Beechinor, S. Lynch, C. NíDheasuna, J.C. Patterson and G.M. Crean, *Appl. Surf. Sci.* **91** (1995) 152.
26. S.K. Roy, S.K. Bose and S.C. Sircar, *Oxid. Met.* **35** (1991) 1.
27. S.-Y. Lee, S.-H. Choi and C.-O. Park, *Thin Solid Films* **359** (2000) 261.
28. J.C. Yang, B. Kolasa and J.M. Gibson, *Appl. Phys. Let.* **73** (1998) 2841.
29. M. Rauh, H.-U. Finzel and P. Wissmann, *Z. Naturforsch.* **54a** (1999) 117.
30. O. Forsén, P. Personen, J. Aromaa and T. Sourtti, *Trans. IMF* **75** (1997) 65.
31. H. Wieder and A.W. Czanderna, *J. Appl. Phys.* **37** (1966) 184.
32. P.K. Krishnamoorthy and S.C. Sircar, *Oxid. Met.* **2** (1970) 349.
33. R. Schennach, M.Y.A. Mollah, J.R. Parga and D.L. Cocke, in Proceedings of XXII Congresso Internaciaonal de Metalurgia y Materiales, November 2000, (Instituto Technologico de Saltillo, Saltillo, Coahuila, Mexico) 122.
34. H. Bubert, E. Grallath, A. Quentmeier and M. Wielunski, *Fresenius J. Anal. Chem.* **353** (1995) 456.
35. D.E. Mencer, M.A. Hossain, J.R. Parga and D.L. Cocke, *J. Mat. Sci. Lett.* **21** (2002) 125.
36. D.E. Mencer, M.A. Hossain, J.R. Parga and D.L. Cocke, *J. Mat. Sci. Lett.* **21** (2002) 1143.
37. M.A. Hossain, D.E. Mencer, M. Kesmez, R. Schennach, M.Y.A. Mollah, D.G. Naugle and D.L. Cocke, unpublished data.
38. N. Bellakhal, K. Draou and J.L. Brisset, *J. Appl. Electrochem.* **27** (1997) 414.
39. D.E. Mencer, Jr., D.L. Cocke and C. Yoon, *Surf. Int. Anal.* **17** (1991) 31.
40. D.L. Cocke, M.S. Owens and R.B. Wright, *Appl. Surf. Sci.* **31** (1988) 341.
41. D.L. Cocke and M.S. Owens, *Appl. Surf. Sci.* **31** (1988) 471.
42. D.L. Cocke, G. Liang, M. Owens, D.E. Halverson and D.G. Naugle, *Mater. Sci. Eng.* **99** (1988) 497.
43. D.L. Cocke, M.S. Owens and R.B. Wright, *Langmuir.* **4** (1988) 1311.
44. D.L. Cocke and M.S. Owens, *J. Colloid and Interf. Sci.* **19** (1989) 166.
45. D.L. Cocke, T.R. Hess, T. Mebrahtu, D.E. Mencer, Jr. and D.G. Naugle, *Solid State Ionics*, **43** (1990) 119.
46. T. Mebrahtu, T.R. Hess, D.E. Mencer, Jr., K.G. Balke, D.G. Naugle and D.L. Cocke, *Mater. Sci. Eng.* **A134** (1991) 1041.
47. D.E. Mencer Jr., T.R. Hess, T. Mebrahtu, D.L. Cocke and D.G. Naugle, *J. Vacuum Sci. Tech.* **A9** (1991) 1610.
48. J.M. Bailey and I.M. Ritchie, *Oxid. Met.* **30** (1988) 405.
49. J.M. Bailey and I.M. Ritchie, *Oxid. Met.* **30** (1988) 419.
50. V.P. Parkhutik, *J. Phys. D: Appl. Phys.* **25** (1992) 256.
51. C. Yoon, 'A Surface Segregation and Oxidation Study of Alloys With Unique Electronic Properties-Implications in Catalysis and Corrosion', Dissertation, Texas A & M University, 1986.
52. T.A. Delchar and F.C. Tompkins, *Proc. R. Soc. London* **A300** (1967) 141.
53. A. Srinivasan, K, Jagannathan, M.S. Hedge and C.N.R. Rao, *Indian J. Chem.* **18A** (1979) 463.
54. C.N.R. Rao, D.D. Sarma and M.S. Hedge, *Proc. R. Soc. London* **A370** (1980) 269.
55. M.J. Braithwaite, R.W. Joyner and M.W. Roberts, *J. Chem. Soc. Faraday Diss.* **60** (1975) 89.
56. D.E. Mencer, 'Preparation and Characterization of Strongly Interacting Amorphous and Polycrystalline Alloys: AgMn and TiAl', Dissertation, Texas A&M University, 1991.
57. D.E. Mencer, T.R. Hess, T. Mebrahtu, J. Patschieder, D.G. Naugle, and D.L. Cocke, *J. Chem. Soc. Chem. Commun. Issue* **22** (1990) 1602.